

P- AND S-WAVE VELOCITY STRUCTURE OF THE CRUST AND UPPER MANTLE UNDER CHINA AND SURROUNDING AREAS FROM BODY AND SURFACE WAVE TOMOGRAPHY

M. Nafi Toksöz, Robert D. van der Hilst, Youshun Sun, Chang Li, and Huajian Yao

Massachusetts Institute of Technology

Sponsored by Air Force Research Laboratory

Contract No. FA8718-04-C-0018

ABSTRACT

The objective of this project is to use a combination of travel-time and surface wave tomography to obtain compressional and shear wave velocity distributions in the crust and upper mantle under China and surrounding areas.

For travel-time tomography, we took a two-step approach. First, we determined three-dimensional (3-D) P- and S-wave velocity structures for the crust and uppermost mantle using local and regional arrival time data. Travel data from the Annual Bulletin of Chinese Earthquakes (ABCE) and the International Seismological Centre (ISC/EHB) are used. A total of 345,000 P-wave, and a similar number of S-wave, arrival times are used for the tomographies. Tomographic inversions provide 3-D P- and S-wave velocities in the crust, P_n and S_n velocities, and Moho depths under China.

To extend the model deeper into the mantle through the upper mantle transition zone, ISC/EHB data for P and PP phases are combined with the ABCE data. To counteract the “smearing effect,” the crust and upper mantle velocity structures, derived from regional travel times, are used. An adaptive grid method based on ray density is used in the inversion. A P-wave velocity model extending down to a depth of 1700 km is obtained. The combined regional-teleseismic tomography provides a high-resolution, 3-D P-wave velocity model for the crust, upper mantle, and the transition zone. The crustal models correlate well with geologic and tectonic features. The mantle models show the images of current and past subduction zones. A surprising result is that the “roots” of some geologic features, such as the Sichuan Basin and Ordos Plateau, extend deep into the upper mantle.

Using surface wave data from broadband stations, the S-velocity structure was determined. Multi-mode surface wave tomography was employed for the whole region of China and surrounding areas. In Tibet, where data from dense networks deployed by Massachusetts Institute of Technology (MIT) and Lehigh University arrays are available, 3-D S-wave velocity structures for the crust and uppermost mantle were obtained using ambient noise interferometry.

OBJECTIVES

The primary goal of this project is to obtain compressional and shear wave velocity distributions in the crust and upper mantle under China and surrounding areas using a combination of travel-time and surface wave tomography.

RESEARCH ACCOMPLISHED

Introduction

China and the surrounding area is a seismically active and geologically complex region (Figure 1). More than 500 earthquakes with magnitudes (M) greater than 6.0 occurred in this region between January 1978 and May 2004 (Sun and Toksöz, 2006). In this paper we present a 3-D compressional and shear wave velocity structure for the crust and upper mantle under China and surrounding regions, obtained using local and regional travel times and surface waves.

The available P- and S-wave velocity models of the crust and upper mantle in China and the surrounding area have been obtained using different approaches. Global models such as CUB 1.0 (Shapiro and Ritzwoller, 2002) and the SAIC $1^\circ \times 1^\circ$ model (Stevens et al., 2001) were constructed from group and phase velocity dispersion measurements of surface waves. The global model CRUST 2.0 (Laske et al., 2001) was constructed from seismic refraction data and developed from the CRUST 5.1 model (Mooney, 1998) and a $1^\circ \times 1^\circ$ sediment map (Laske and Masters, 1997). Only P-wave velocities are inverted by travel-time tomography. The S-wave velocities in the model are obtained by empirical V_p/V_s ratios or compiled from other sources. For East Asia, mantle S-velocity models were obtained from shear and surface waveforms (Friederich, 2003). Lateral spatial resolution of the models is larger than 200 km.

Regional models were constructed by S_n and/or P_n tomography (Ritzwoller et al., 2002; Hearn and Ni, 2001; Pei et al., 2007), and from surface waves (e.g., Wu et al., 1997; Lebedev and Nolet, 2003; Huang et al., 2003). P- and S-wave tomographies have been performed in several local regions in China (e.g., Huang and Zhao, 2004). All these models provide detailed crustal structures in specific regions. A detailed map for the whole China area remains to be developed.

In this study, using both travel-time body and surface wave tomography, we produce multi-scale, 3-D P- and S-wave velocity models for the crust, upper mantle, and transition zone. In the following sections we describe the data, P- and S-wave travel-time tomography, long wavelength surface wave tomography, and array tomography, respectively.

Data for Travel-Time Tomography

The P- and S-wave arrival times from local, regional, and global stations come from four sources: (1) ABCE Phase readings from about 220 stations of the Chinese Seismograph Network (CSN) during the period 1990-2004 (IG-CSB [Institute of Geology, Chinese Seismological Bureau], 1990-2004) (Figure 1); (2) EHB (Engdahl, van der Hilst, and Buland, 1998) data reprocessed from the International Seismological Centre (ISC) bulletins (1964–2004); (3) PP-P differential times, used to image the upper mantle beneath regions with few earthquakes and stations; and (4) broadband waveform data, used for surface wave tomography and for model validation using synthetic seismograms.

Combining the global, regional, and local seismic network data from various sources requires careful processing in order to avoid internal inconsistencies. The travel time picks from source 1 above have been integrated and processed along with data from source 2 (i.e., the existing EHB data) using a non-linear process of earthquake relocation and phase re-identification (Engdahl et al., 1998). Most baseline inconsistencies can simply be removed by recalculating all new picks relative to EHB hypocenters using ak135 travel time.

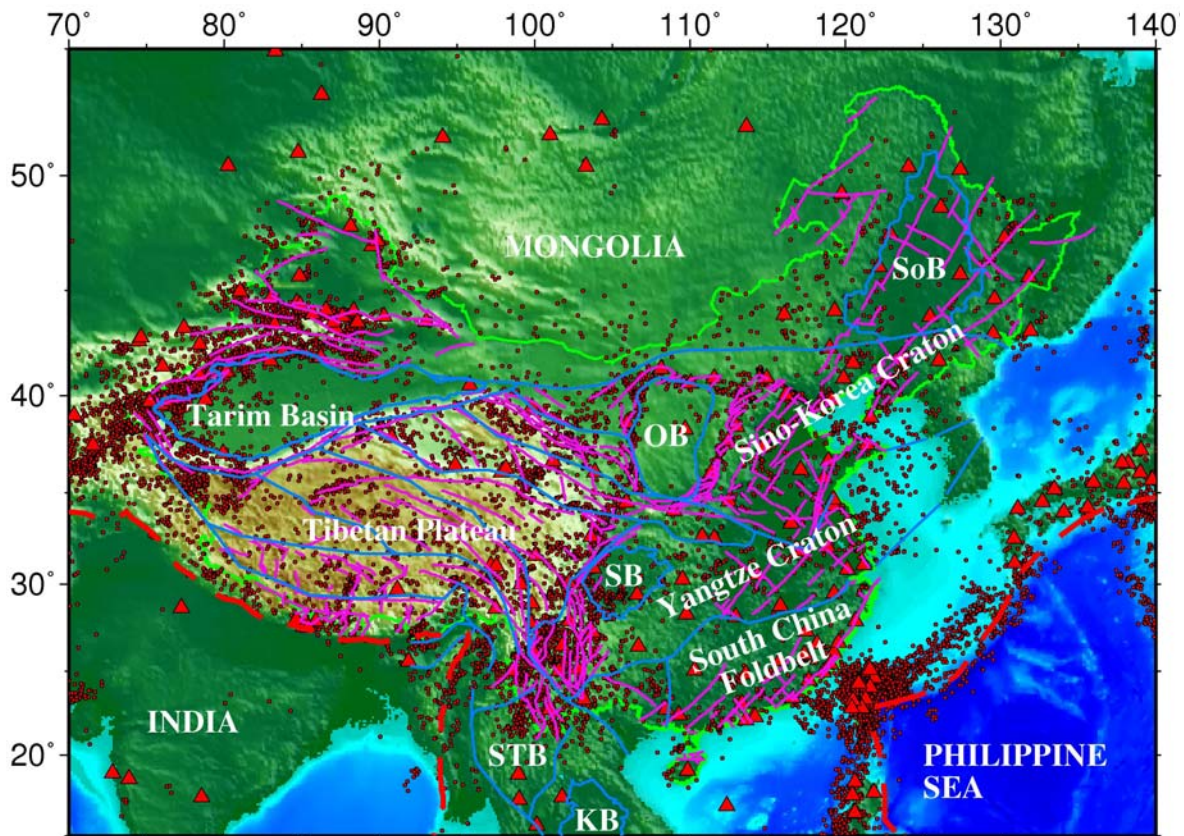


Figure 1. Shown are 25,000 earthquakes ($M > 3.0$ from 1990 to 2004), 220 stations, active faults, and major tectonic boundaries in China and the surrounding area. Earthquake epicenters are shown in red dots, and stations are shown in red triangles. The yellow line shows the boundary of China. Active faults in the China area are shown in purple lines, and tectonic sutures are shown in blue lines, where SoB is Songliao Basin; OB is Ordos Basin; SB is Sichuan Basin; KB is Khorat Basin; STB is Shan Thai Block; and IB is Indochina Block.

P- and S-Wave 3-D Velocity Models from Travel-Time Tomography

The tomography research used here builds on our team's extensive experience in travel-time tomography for the crust and mantle (van der Hilst et al., 1991; Káráson and van der Hilst, 2001; Sun et al., 2004; Li et al., 2006; Sun and Toksöz, 2006; Li, 2007; Sun et al., 2007). We took a two-step approach. First, we determined 3-D velocity structures for the crust and uppermost mantle (P_n , S_n). Second, we conducted the mantle tomography with the travel-times calculated from crustal models used as inputs, in order to reduce the "smearing" effect of shallow velocity structure on steep rays. In the proposed project we will follow a similar approach.

Crust and uppermost mantle P- and S-wave velocities

A high-resolution tomographic model for the heterogeneous crust is constructed by iterative, non-linear tomography. To generate adequate starting models for the non-linear inversion we combine pertinent information from global (Mooney, 1998; Bassin et al., 2000; Stevens et al., 2001; Ritzwoller et al., 2002), regional and local crust, and uppermost mantle models (Wang et al., 2003; Sun et al., 2004; Huang and Zhao, 2006; Li et al., 2006; Reiter and Rodi, 2006; Sun and Toksöz, 2006; Yao et al., 2006), in addition to P_n or S_n studies (Hearn and Ni, 2001; Hearn et al., 2004; Liang et al., 2004; Phillips et al., 2005; Rowe et al., 2005) and seismic refraction profiles (Morozov et al., 2005; Li, Mooney, and Fan, 2006). Next, we use the adaptive moving window (AMW) approach (Sun et al., 2004) to obtain crustal velocities and P_n and S_n models from a one-dimensional (1-D) Monte Carlo inversion of local ($\leq 20^\circ$) arrival time data in the whole region, building these into the next model (Model #2).

The third step is a tomographic inversion of the local and regional arrival time data for 3-D variations in the P- and S-wave speed, using Model #2 as the initial input model.

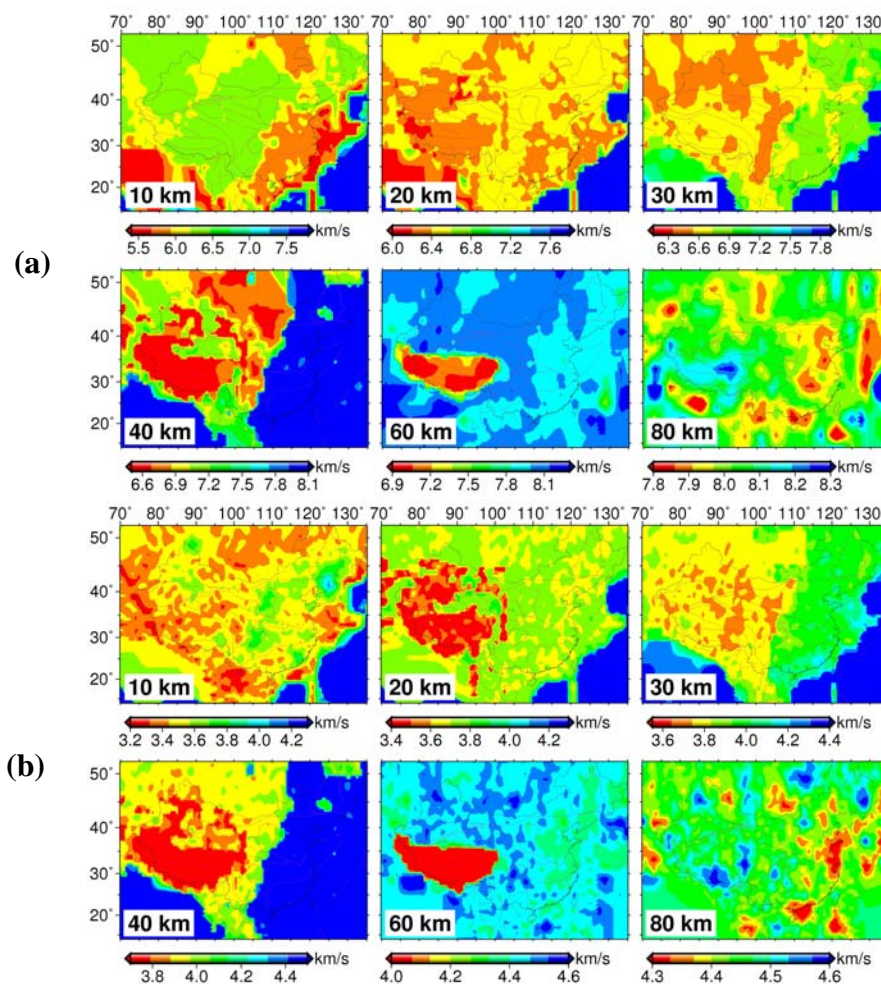


Figure 2. Horizontal slices of three-dimensional (a) V_p and (b) V_s models for China and surrounding regions at 10, 20, 30, 40, 60, and 80 km depths.

For this purpose we use a modified version of Zhao’s tomographic method (Zhao et al., 1992; Sun and Toksöz, 2006), which allows for 3-D velocity variations everywhere in the model and can accommodate velocity discontinuities. The velocity structure is discretized using a 3-D grid. The velocity perturbation at each point is calculated by linear interpolation of the velocity perturbations at surrounding (adjacent) grid nodes. The velocity perturbations at grid nodes are the unknown parameters for the inversion procedure. To calculate travel-times and ray paths accurately and rapidly, the pseudo-bending technique (Um and Thurber, 1987) and Snell’s law are used iteratively. We correct for station elevations by including station correction terms in the inversion. The LSQR algorithm (Paige and Saunders, 1982), with regularization, is used to solve the large and sparse system of equations. The non-linear tomographic problem is solved by repeated linear inversions. At each iteration, perturbations to hypocentral parameters and velocity structure are determined simultaneously.

P- and S-wave velocity tomograms obtained for China and surrounding areas, using this method, are shown in Figures 2 and 3. The 3-D velocity model reduces the residuals and event location errors. For example, for 11 explosions at the Lop Nor site, relocation with our 3-D models reduced hypocenter errors to 1 km or less (Sun and Toksöz, 2006, Table 2).

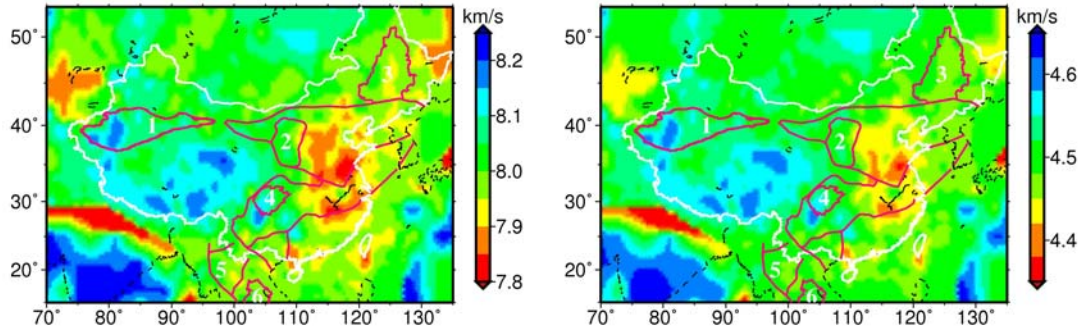


Figure 3. P_n (left) and S_n (right) velocities in China and surrounding regions. 1. Tarim Basin; 2. Ordos Basin; 3. Songliao Basin; 4. Sichuan Basin; 5. Shan Thai Block; and 6. Khorat Basin.

Mantle tomography

For the upper mantle tomography, we use the multi-scale travel-time methodology we developed and improved over 15 years (e.g., van der Hilst et al., 1991; Kárason and van der Hilst, 2001; Li et al., 2006). Even though we focus on accurate imaging of mantle structure beneath East Asia, we perform global inversions in order to avoid artifacts created by wave propagation through the structure outside the mantle volume that is of interest here. To mitigate effects of uneven data coverage, we adapt the size of the grid block to the sampling density of the high frequency data (Kárason and van der Hilst, 2000). The size of the blocks is a multiple of 45 km x 0.35° x 0.35° (in depth, latitude, and longitude) beneath the study region (down to 800 km depth) and 45 km x 0.7° x 0.7° elsewhere. To reduce artifacts created by strong crust heterogeneity that cannot be resolved upon linearized inversion for mantle structure, we apply a crust correction using the crust models resulting from the non-linear tomography described in the previous section.

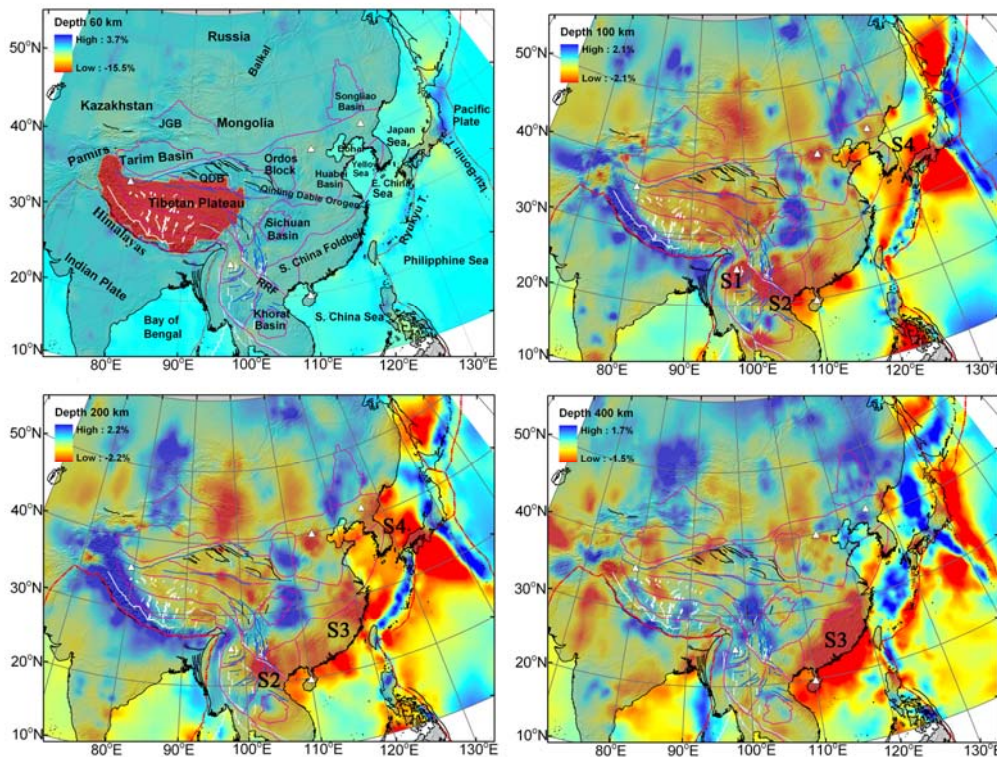


Figure 4. Lateral P-wave speed perturbations at 60, 100, 200, and 400 km depths.

We use, again, the iterative LSQR algorithm to minimize an objective function combining a measure of data misfit and regularization terms:

$$\varepsilon = \|\mathbf{Gm} - \mathbf{d}\|^2 + \lambda_1 \|\mathbf{m}\|^2 + \lambda_2 \|\mathbf{Lm}\|^2 + \lambda_3 \|\mathbf{C} - \mathbf{m}_c\|^2. \quad (1)$$

In the first term, \mathbf{m} represents the model vector, including the constant slowness perturbation in each grid cell as well as hypocenter perturbation terms. \mathbf{G} is the sensitivity matrix, calculated using ray theory for the short period data and 3-D finite frequency kernels estimated from single scattering for long period data measured by waveform cross-correlation (Káráson, 2002). The data vector \mathbf{d} represents the travel-time residuals. The second and third terms are traditional Tikhonov regularizations that produce “minimum structure” models consistent with the data. The second term represents “norm damping” and favors a result that is close to the reference model (it minimizes the amplitude of the model). The third term reduces the difference between adjacent cells and thus produces smooth variations; L is a first order differential operator. λ_1 and λ_2 are the weights of Tikhonov regularization.

The last term in (1) is used to prevent time delays accrued in highly heterogeneous crust from producing artifacts in the mantle model (Li et al., 2006), with \mathbf{C} representing a best *a priori* estimate of the crust model and \mathbf{m}_c representing the crustal part in the model vector \mathbf{m} . The weight λ_3 is determined through synthetic tests (Li et al., 2006). P-wave velocity models obtained for China and surrounding areas by applying this method to a preliminarily assembled data set are shown in Figures 4 and 5.

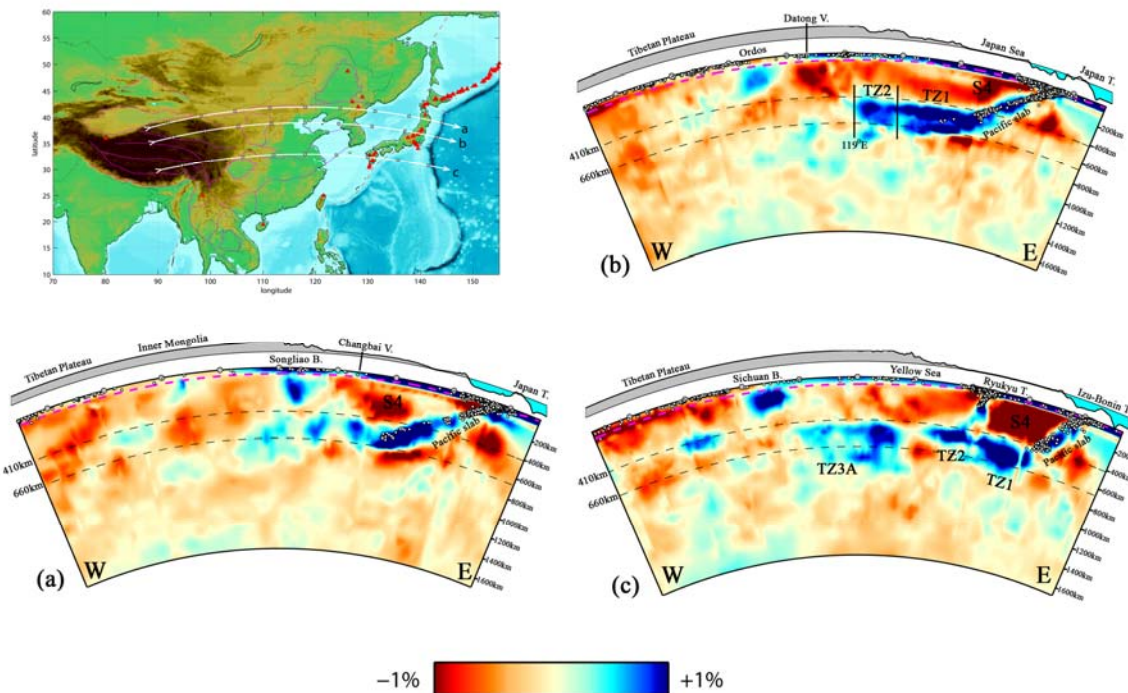


Figure 5. West-east vertical cross-sections (a), (b), and (c) through the 3-D P-wave velocity model (indicated as white lines in the upper left hand image).

Surface Wave Tomography

In addition to estimating S-wave velocities beneath East Asia from tomographic inversion of S-wave travel time data, we use surface waves to further constrain the S-wave velocity models.

Automated multi-mode Surface Wave Tomography

Using multi-mode inversion technology we resolve long wavelength structures in the upper mantle (Lebedev and van der Hilst, 2007). To enable application to the massive volumes of earthquake data now available through international data repositories, Lebedev's multi-mode inversion procedure is almost fully automated. The velocity model for East Asia is shown in Lebedev and van der Hilst (2007). The dense data coverage in China would enable the construction of shear wave velocity models at a substantially higher resolution.

Array Tomography Based on Ambient Noise Interferometry

Where we have dense station coverage we use cross-correlation and ambient noise tomography to obtain shear wave velocity (Campillo and Paul, 2003). We have developed a surface wave array tomography technique that uses phase velocity measurements from the empirical Green's functions (EGF) estimated from the ambient noise interferometry (Yao et al., 2006). Yao et al. (2006) shows, for broadband arrays in southeastern Tibet, the dense path coverage that can be achieved with this technique and the phase velocity at the period of 30 seconds from EGF analysis. Resolution tests suggest that with this data coverage one can resolve shallow mantle structure on length scales as small as ~ 100 km. Figure 6 shows the dense path coverage and lateral variations in S-wave velocity along several cross sections beneath the arrays.

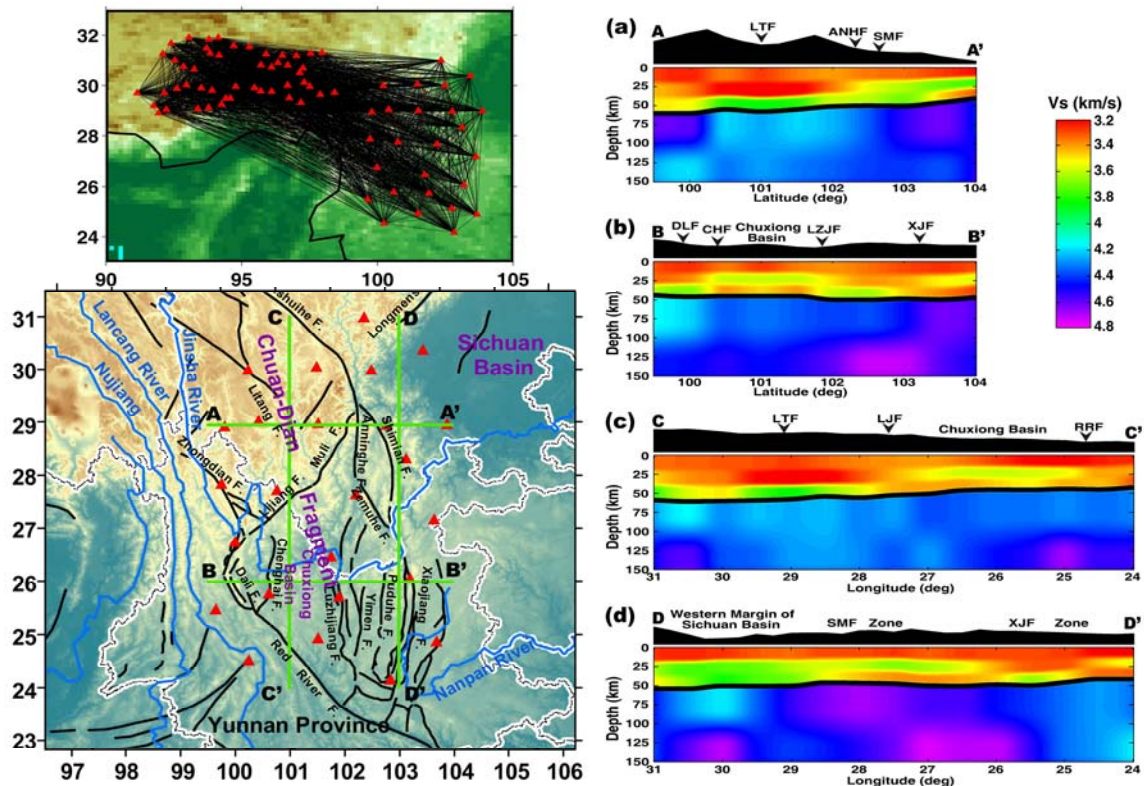


Figure 6. Interstation ray paths (upper left corner) from ambient noise interferometry study for MIT and Lehigh University arrays in southeastern Tibet. Shear wave speeds at four cross-sections through the Sichuan and Yunnan provinces of China from the combined results of ambient noise interferometry study and two-station dispersion analysis.

Because of the relatively short periods involved, using data from ambient noise interferometry alone would only constrain structure in the top half of the continental lithosphere. Therefore, we combine dispersion analysis of the empirical Green's functions from interferometry with constraints from traditional interstation dispersion analysis; together they allow spectral analysis over a wide frequency band (8–100 mHz), which allows resolution of structure between ~ 10 to 150 km depth (Yao et al., 2006, 2007).

CONCLUSIONS AND RECOMMENDATIONS

The 3-D compressional and shear-wave velocity models of the crust and upper mantle, obtained by travel-time and surface wave tomography, reveals pronounced lateral heterogeneities under China and surrounding regions. The velocity models exhibit the following features.

1. At the upper crust, down to 20 km depth, velocity variations strongly correlate with the major geological features.
2. There is a strong contrast between the regions to the east of 110°E longitude and the west. In eastern China, where crustal thickness is about 35 km or less, velocity variations are relatively small. Lower velocities delineate the rift structure of northeastern China. In the region to the west of 110°E longitude, the crustal velocities are much more variable. Crustal thickness varies between 35 km and 78 km. The roots of prominent features such as the Tibet, Tarim, Sichuan, and Ordos basins, dominate the subsurface velocity structures.
3. There is a prominent low velocity zone in the middle crust (around 40 km depth) under central Tibet. Shear velocity decreases by as much as 6% relative to the values north of Tibet and Tarim basin.
4. In general, there is good correlation between the P-wave and S-wave velocity variations. However, relative magnitudes of the variations (i.e., percentage velocity changes) are different in different regions. For example, the shear velocity decrease in the mid-crust under Tibet is twice as large as that of the P-wave velocity, percentage wise.
5. In the upper mantle, the percentage variation of shear velocities is greater than those of P-wave velocities.

Picking of shear wave arrivals is more prone to error than the picking of first arriving P waves, but previous studies have demonstrated the value of the reprocessed (EHB) S travel time residuals for seismic tomography (e.g., Kennett et al., 1998; Widiyantoro et al., 1998). Encouraged by those results, we will attempt travel time tomography for S-wave velocity beneath East Asia. For this purpose we will augment the EHB data with S picks from the 1200 stations of the Chinese Seismograph Network and the networks in Russia.

REFERENCES

- Bassin, C., G. Laske, and G. Masters (2000). The Current Limits of Resolution for Surface Wave Tomography in North America. *EOS Trans AGU* 81: F897.
- Campillo, M. and A. Paul (2003). Long-range correlations in the diffuse seismic coda, *Science*, 299: 547–549.
- Engdahl, E.R., R.D. van der Hilst, and R. Buland (1998). Global teleseismic earthquake relocation with improved travel times and procedures for depth determination. *Bull. Seism. Soc. Am.* 88: 722–743.
- Friederich, W. (2003). The S-velocity structure of the East Asian mantle from inversion of shear and surface waveforms, *Geophys. J. Int.* 153: 88–102.
- Hearn, T.M. and J.F. Ni (2001). Tomography and location problems in China using regional travel-time data, in *Proceedings of 23rd Seismic Research Review: Worldwide Monitoring of Nuclear Explosions*, LA-UR-01-4454, Vol. 1, pp. 27–45.
- Hearn, T. M., S. Wang, J. F. Ni, Z. Xu, Y. Yu, and X. Zhang (2004). Uppermost mantle velocities beneath China and surrounding regions, *J. Geophys. Res.* 109: doi:10.1029/2003JB002874.
- Huang, J., and D. Zhao (2004). Crustal heterogeneity and seismotectonics of the Chinese capital region. *Tectonophysics* 385: 159–180.

29th Monitoring Research Review: Ground-Based Nuclear Explosion Monitoring Technologies

- Huang, J. and D. Zhao (2006). High-resolution mantle tomography of China and surrounding regions, *J. Geophys. Res.* 111: B09305, doi:10.1029/2005JB004066.
- Huang, Z., W. Su, Y. Peng, Y. Zheng, and H. Li (2003). Rayleigh wave tomography of China and adjacent regions, *J. Geophys. Res.* 108: (B2), 2073, doi:10.1029/2001JB001696.
- Kárason, H., and R.D. van der Hilst (2000). Constraints on mantle convection from seismic tomography. In M.A. Richards, R. Gordon and R.D. van der Hilst (Editors), *History and Dynamics of Plate Motion. Am. Geophys. Union, Geophys. Monogr. Ser.* 121: 277–288.
- Kárason, H., and R.D. van der Hilst (2001). Tomographic imaging of the lowermost mantle with differential times of refracted and diffracted core phases (PKP, Pdiff), *J. Geophys. Res.* 106: 6569–6587.
- Kárason, H. (2002). Constraints on mantle convection from seismic tomography and flow modeling, Ph.D. thesis, Massachusetts Institute of Technology, Cambridge, MA.
- Kennett, B.L.N., S. Widiyantoro, and R.D. van der Hilst (1998). Joint seismic tomography for bulk-sound and shear wavespeed, *J. Geophys. Res.* 103: 12469–12493.
- Laske, G., and G. Masters (1997). A global digital map of sediments thickness (abstract), *EOS* 78, F483.
- Laske, G., G. Masters, and C. Reif (2001). CRUST 2.0: a new global crustal model at 2x2 degrees, <http://mahi.ucsd.edu/Gabi/rem.dir/crust/crust2.html> (last accessed July 2005).
- Lebedev, S., and G. Nolet (2003). Upper mantle beneath southeast Asia from S velocity tomography. *J. Geophys. Res.* 108; doi 10.1029/2000JB000073.
- Lebedev, S., and R.D. van der Hilst (2007). Global upper-mantle tomography with the automated multi-mode surface and S waveforms, *Geophys. J. Int.* (under review).
- Li, C. (2007). Evolution of upper mantle beneath East Asia and the Tibetan Plateau from P-wave tomography, Ph.D. thesis, Massachusetts Institute of Technology, Cambridge, MA.
- Li, C., R.D. van der Hilst, and M. N. Toksoz (2006). Constraining P-wave velocity variations in the upper mantle beneath Southeast Asia, *Phys. Earth Planet. Inter.* 154: 180–195.
- Li, S.L., W.D. Mooney, and J. Fa, (2006). Crustal structure of mainland China from deep seismic sounding data, *Tectonophysics* 420: 239–252.
- Liang, C., X. Song, and J. Huang (2004). Tomographic inversion of Pn traveltimes in China, *J. Geophys. Res.* 109: B11304, doi:10.1029/2003JB002789.
- Mooney, W. D. (1998). CRUST 5.1: a global crustal model at 5° x 5°. *J. Geophys. Res.* 103: 727–747.
- Morozov, I.B., E.A. Morozova, S.B. Smithson, P.G. Richards, V.I. Khalturin, and L.N. Solodilov (2005). 3D first-arrival regional calibration model of northern Eurasia, *Bull. Seism. Soc. Am.* 95: 951–964.
- Paige, C., and M. Saunders (1982). LSQR: An algorithm for sparse linear equations and sparse least squares. *ACM Trans. Math. Software* 8: 471.
- Pei, S., J. Zhao, Y. Sun, Z. Xu, S. Wang, H. Liu, C. A. Rowe, M. N. Toksöz, and X. Gao (2007). Upper mantle seismic velocities and anisotropy in China determined through Pn and Sn tomography. *J. Geophys. Res.* 112: B05312, doi:10.1029/2006JB004409.
- Phillips, W. S., C. A. Rowe, and L. K. Steck (2005). The Use of interstation arrival time differences to account for regional path variability, *Geophys. Res. Letts.* 32; L11301, doi:10.1029/2005GL022558.

29th Monitoring Research Review: Ground-Based Nuclear Explosion Monitoring Technologies

- Reiter D. and Rodi W. (2006). Crustal and Upper-mantle P- and S- velocity structure in central and southern Asia form joint body -and surface- wave inversion, in *Proceedings of the 28th Seismic Research Review: Ground-Based Nuclear Explosion Monitoring Technologies*, LA-UR-06_5471, Vol. 1, pp. 209–218.
- Ritzwoller, M. H., M. P. Barmin, A. Villasenor, A. L. Levshin, and E. R. Engdahl (2002). Pn and Sn tomography across Eurasia to improve regional seismic event locations. *Tectonophysics* 358; 39–55.
- Rowe, C, Steck, L. K., W. S. Phillips, M. Begnaud, R. Stead, and H. Hartse (2005). Pn tomography and location in Eurasia, 2005 IASPEI Meeting, Santiago, Chile.
- Shapiro, N. M., and M. H. Ritzwoller (2002). Monte Carlo inversion for a global shear velocity model of the crust and upper mantle. *Geophys. J. Int.* 151: 88–105.
- Stevens, J. L., D. A. Adams, and G. E. Baker (2001). Improved surface wave detection and measurement using phase-matched filtering with a global one-degree dispersion model, in *Proceedings of the 23rd Seismic Research Review: Worldwide Monitoring of Nuclear Explosions*, LA-UR-01-4454, Vol. 1, pp. 420–430.
- Sun, Y. and M.N. Toksöz (2006). Crustal structure of China and surrounding regions from P wave traveltimes tomography, *J. Geophys. Res.* 111: B03310, doi:10.1029/2005JB003962.
- Sun, Y., X. Li, S. Kuleli, F. D. Morgan, and M. N. Toksöz (2004). Adaptive moving window method for 3-D P-velocity tomography and its application in China. *Bull. Seism. Soc. Am.* 94: 740–746.
- Sun, Y., M.N. Toksöz, S. Pei, and D. Zhao (2007). S-wave Tomography of the Crust and uppermost mantle in China. In preparation for submission to *J. Geophys. Res.*
- Um, J., and C. Thurber (1987). A fast algorithm for two-point seismic ray tracing. *Bull. Seism. Soc. Am.* 77: 972–986.
- Van der Hilst, R.D., E.R. Engdahl, W. Spakman, and G. Nolet (1991) Tomographic imaging of subducted lithosphere below northwest Pacific island arcs, *Nature* 353: 37–42.
- Wang, C.-Y., W. W. Chan, and W. D. Mooney (2003). Three-dimensional velocity structure of crust and upper mantle in southwestern China and its tectonic implications, *J. Geophys. Res.* 108: (B9), 2442, doi:10.1029/2002JB00.
- Widiyantoro, S., B.L.N. Kennett, and R.D. van der Hilst (1998). Extending shear-wave tomography for the lower mantle using S and SKS arrival-time data, *Earth, Planets, and Space* 50: 999–1012.
- Wu, F. T., A. L. Levshin, and V. M. Kozhevnikov (1997). Rayleigh wave group velocity tomography of Siberia, China, and vicinity. *Pure Appl. Geophys.* 149: 447–473.
- Yao, H., R.D. van der Hilst, and M.V. De Hoop (2006). Surface-wave array tomography in SE Tibet from ambient seismic noise and two-station analysis: I - Phase velocity maps, *Geophys. J. Int.* 166: 732–744, doi: 10.1111/j.1365-246X.2006.03028.x.
- Yao, H., C. Beghein, and R.D. van der Hilst (2007). Surface-wave array tomography in SE Tibet from ambient seismic noise and two-station analysis: II –crustal and upper mantle structure, submitted to *Geophys. J. Int.*
- Zhao, D., A. Hasegawa, and S. Horiuchi (1992). Tomographic imaging of P and S wave velocity structure beneath northeastern Japan. *J. Geophys. Res.* 97 19909–19928.